Multiscale wavelet analysis of 3D Lagrangian trajectories in a mechanically agitated vessel

Savari, Chiya; Li, Kun; Barigou, Mostafa

DOI:
10.1016/j.ces.2022.117844

Chemical Engineering Science 260 (2022) 117844

Contents lists available at ScienceDirect

Chemical Engineering Science

journal homepage: www.elsevier.com/locate/ces

Multiscale wavelet analysis of 3D Lagrangian trajectories in a mechanically agitated vessel

Chiya Savari, Kun Li, Mostafa Barigou *

School of Chemical Engineering, University of Birmingham, Edgbaston, Birmingham B15 2TT, UK

HIGHLIGHTS

- 3D Lagrangian flow trajectories are determined in a mechanically agitated vessel.
- A new multiscale wavelet analysis is used to study turbulence properties.
- Trajectories are decomposed into deterministic and stochastic components.
- Decomposed trajectories yielded turbulence kinetic energy and its dissipation rate.
- The stochastic trajectory component yielded the turbulence diffusion coefficients.

ARTICLE INFO

Article history:
Received 12 May 2022
Received in revised form 23 June 2022
Accepted 27 June 2022
Available online 2 July 2022

Keywords:
Agitated vessel
Mixing
Turbulence
Turbulent kinetic energy
Dissipation rate
Eddy diffusivity

ABSTRACT

Flow turbulence properties are of utmost importance for the optimization of mixing in stirred vessels. A new experimental-theoretical framework is developed to study such turbulence properties. A discrete wavelet transform is used to decompose Lagrangian flow trajectories measured by positron emission particle tracking into their mean and stochastic components representing different scales. The mean component represents low frequency scale motion or non-diffusive/background motion, while the stochastic component accounts for high frequency scale motion or diffusive motion of small eddies. Decomposed Lagrangian trajectories are used to construct maps of local mean and fluctuation flow velocity, turbulent kinetic energy and its dissipation rate, and, for the first time, turbulent diffusion coefficients. Particle image velocimetry measurements are utilised to independently validate results and tune the input parameters of the analysis. Such detailed information on local mixing scales is invaluable to aid equipment design and operation and facilitate heat/mass transfer and enhance reaction kinetics.

1. Introduction

Mechanically agitated vessels operating in the turbulent regime are extensively used in various industries such as chemical, biochemical, pharmaceutical, crystallization, minerals, food, and dissolution (Shah et al., 2015). Mixing quality or mixedness in this type of equipment is of paramount importance in determining process reliability, product quality and cost. To properly design mixing units, knowledge of flow turbulence characteristics such as turbulent kinetic energy (TKE) and its dissipation rate are required, as the spatial distribution and magnitude of these parameters determines the efficiency and quality of the mixing process. It is generally difficult to obtain these turbulence properties as it is hard to conduct pointwise experimental investigations of the internal flow within mixing vessels due to its complexity. A lack of proper understanding of mixing hydrodynamics may cause severe manufacturing problems costing billions of dollars per year (Paul et al., 2003). Therefore, proper and accurate combined experimental and theoretical approaches to characterise turbulence properties in stirred vessels to help evaluate mixing quality are of crucial importance.

Over the years, several experimental methods have been developed for measuring TKE and its dissipation rate. Traditionally, the dissipation rate of TKE is measured using a hot-wire probe which is based on the heat loss of an electrically heated wire (Antonia, 2003; Wallace and Vukoslavčević, 2010; Zhu and Antonia, 1996). This technique directly measures the dissipation rate; however, it is an invasive technique and it needs multiple hot-wire probes to measure all 3D velocity components and their gradients, which can significantly perturb the flow (Wallace and Vukoslavčević, 2010). Other measurement techniques are laser-based optical

* Corresponding author.
E-mail address: m.barigou@bham.ac.uk (M. Barigou).

https://doi.org/10.1016/j.ces.2022.117844
0009-2509/

Nomenclature

Symbols

A_j	approximate sub-signal at j-th level
b	constant in turbulent diffusion coefficient equation
c	concentration, mol/m^3
$\bar{c}$	mean concentration, mol/m^3
C_{imp}	impeller clearance, m
D	impeller diameter, m
D_j	detail sub-signal at j-th level
D_m	molecular diffusion coefficient, m^2/s
f_s	sampling frequency
H	liquid height in the tank, m
k	turbulent kinetic energy or TKE, m^2/s^2
K	turbulent diffusion coefficient, m^2/s
n	length of time series
N	impeller rotational speed, 1/s
N_p	power number
P	input power, W
r	radial position, m
R	tank radius, m
Re_{imp}	impeller Reynolds number
t	time, s
T	tank diameter, m
u	instantaneous velocity, m/s
u_p	periodic fluctuation velocity, m/s
u'	fluctuation velocity, m/s
u''	pure random fluctuation velocity, m/s
U_{rz}	r-z velocity, m/s
U_{3D}	total velocity, m/s
U_{tip}	impeller tip velocity, m/s
V_l	tank volume, m^3
w	baffle width, m
W	impeller width, m
x	x-direction position, m
x_{det}	x-direction deterministic Lagrangian displacement, m
x_{sto}	x-direction stochastic Lagrangian displacement, m
y	y-direction position, m
z	z-direction position, m

Greek Symbols

δ	standard deviation of fluctuation velocity, m/s
ε	turbulent kinetic energy dissipation rate, m^2/s^3
$\bar{\varepsilon}$	mean turbulent kinetic energy dissipation rate, m^2/s^3
μ	viscosity, kg/ (m.s)
ν	kinematic viscosity, m^2/s
ρ	liquid density, kg/m^3
σ	standard deviation of stochastic Lagrangian displacements, m
ψ	wavelet mother function

Abbreviations

DWT	discrete wavelet transform
LDV	laser Doppler velocimetry
PBT	pitched-blade turbine
PEPT	positron emission particle tracking
PIV	particle image velocimetry
TKE	turbulent kinetic energy

imaging techniques such as laser Doppler velocimetry (LDV) and particle image velocimetry (PIV). LDV measures local, instantaneous flow velocities in transparent media using the Doppler shift principle in a laser beam scattered by seeding particles suspended in the flow (Tropea, 1995). For example, Zhou and Kresta (1996) used 1D LDV to study the influence of vessel geometry on the maximum TKE dissipation rate. They reported that 28.1% of the turbulent energy is dissipated in the discharge plane of the impeller. Several other researchers employed dimensional analysis to indirectly estimate the turbulent dissipation rate distributions in agitated vessels (Boffetta and Romano, 2002; Kresta and Wood, 1993; Schäfer et al., 1997), while some workers directly measured the energy dissipation rate using 2-point 4-channel LDV, with 9 out of 12 mean squared velocity gradients (Ducci and Yianneskis, 2005; La Forgia et al., 2019).

PIV is widely accepted and gives non-invasive Eulerian measurements based on the spatial averaging of small tracer displacements between images (Adrian, 1991). Most researchers have used 2D flow velocity fields and very few workers have used stereo-PIV to evaluate the local TKE distribution, its mean and dissipation rate (Gabriele et al., 2011; Guida et al., 2010a; Mortensen et al., 2018; Sharp and Adrian, 2001; Stanislas et al., 2008). The accuracy of turbulence properties measured by PIV is mainly determined by the spatial resolution. It is hard to have a high spatial resolution in PIV measurements due to noise in the data, hence, the measured flow properties at high resolution may be well overestimated due to noise amplification (Tanaka and Eaton, 2007). Although, some efforts have been devoted to increasing the temporal and spatial resolution by using 3D PIV (Tao et al., 2000, 2002; Zeff et al., 2003), the applicability to measure turbulence properties is still limited by the complexity of the technique and associated data analysis. Despite their advantages, laser-based optical image techniques suffer from flow transparency constraint, which limits their application of these techniques to real industrial flows which tend to be opaque. Therefore, the use of an experimental measurement technique which can be used in opaque flows is of utmost importance for extracting turbulence properties. Positron emission particle tracking (PEPT) is an experimental measurement technique which can provide 3D Lagrangian trajectories of flow in opaque systems (Fangary et al., 2002; Guida et al., 2010b). A tiny radiolabelled tracer is used as a flow follower which can be tracked in 3D space and time, thus, revealing the long-term Lagrangian trajectory of the fluid which can be used to extract the turbulence properties of the flow.

Turbulent fluid mixing in mechanically agitated tanks takes place at different scales, i.e., molecular, eddy and bulk scales. As such, it can be treated as a multiscale problem involving micro- and macromixing. Turbulent flow in agitated tanks consists of eddies of different scales, whereby the largest eddies have a size of the same order of magnitude as the rotating impeller, while the finest eddies have sizes defined by the Kolmogorov length scale. Larger eddies give rise to smaller eddies, so that kinetic energy is cascaded down from large-scale eddies to small ones. Viscosity predominates at the smallest scales and energy is dissipated as heat (Argoul et al., 1989). Mixing on the largest scales, i.e., macromixing, is characterized by bulk fluid motion and reflects how quickly an added substance is dispersed in the volume of the tank. On the other hand, micromixing occurs via small eddies and molecular diffusion, causing homogeneity of scalar entities. The identification of these mixing scales is of significant industrial relevance as macromixing determines the blending time and micromixing affects the transfer of heat and mass as well as reaction rates.

As advocated above, a combined theoretical–experimental approach is necessary for estimating the flow turbulence properties in agitated tanks. While an accurate experimental method is

crucial for determining turbulence characteristics, an appropriate theoretical technique is also critical for experimental data analysis. Lagrangian trajectories provided by PEPT contain abundant 3D flow information which can be used to infer a detailed description of the mixing scales in the vessel. Such trajectories consist of deterministic displacements (low frequencies) and stochastic ones (high frequencies). The deterministic part represents the mean or background flow motion, while the stochastic part accounts for the movement of small-scale fluid parcels. Decomposing the flow Lagrangian trajectories into deterministic and stochastic parts can provide valuable information on the degree of macro as well as micromixing. Wavelet analysis is a powerful and well-established technique in the field of signal processing. It can elucidate the localized characteristics of a signal both in temporal and frequency domains. Mallat (1989) developed one of the most reliable decomposition techniques implementing wavelet analysis called discrete wavelet transform (DWT). The method is based on a convolution between the original signal and two filters, a high-pass and a low-pass filter. Outputs of this transform consist of a series of decomposed sub-signals at different scales, giving a multiresolution representation of the signal. DWT has been used to analsye time series signals in different fields such as engineering (Ellis et al., 2003; Guenther and Breault, 2007; Wu et al., 2013), oceanography (Thiebaut and Vennell, 2010; Thomson and Emery, 2014), biology (Babichev et al., 2018; Xiong et al., 2015) and medicine (Addison, 2017; Lyashenko et al., 2016), but it has not been used to study the dynamics of flow systems such as stirred vessels.

In this work, a new accurate multiscale analysis of long-term PEPT Lagrangian trajectories based on discrete wavelet decomposition is used to describe the different mixing scales in a single-phase mechanically agitated tank. The trajectories are decomposed into their deterministic and stochastic parts, which are then used to estimate the local mean (background) and fluctuating velocity flow maps, local turbulent kinetic energy and its dissipation rate, and local eddy diffusivities. Moreover, local velocity measurements acquired via a PIV technique are used to independently validate the results and tune the input parameters of the multiscale analysis. Detailed information on the mixing scales and turbulence properties are obtained, enabling regions with different mixing scales to be identified.

2. Experimental section

2.1. Apparatus

Mixing experiments were performed in a standard-configuration mechanically agitated cylindrical tank with diameter T = 0.19 m, as shown in Fig. 1. The tank was filled with water to a height $H = T$ and the impeller was a pumping-down 6-blade 45° pitched-blade turbine (PBT), having diameter D = 0.5 T, width W = 0.1 T and off-bottom clearance C_{imp} = 0.33 T. The tank was equipped with four wall baffles of width w = 0.1 T. The impeller rotational speed was N = 3.67 s^{-1} corresponding to an impeller Reynolds number ($Re_{imp} = \rho ND^2/\mu$) of 40000, thus, ensuring fully turbulent flow.

2.2. PEPT experiments

PEPT is a non-invasive measurement technique which uses a single tiny positron-emitting-tracer particle to track a liquid or a solid phase and provide its 3D long-term Lagrangian trajectory within a of flow setup (Barigou, 2004). PEPT has the advantage of being able to diagnose flow in opaque systems which circumvents the transparency constraint of optical visualisation methods. PEPT is a well-established technique and has been extensively used to investigate single and multiphase flows inside agitated vessels and pipes (Barigou, 2004; Eesa and Barigou, 2008, 2009; Fairhurst et al., 2001; Guida et al., 2012; Li et al., 2022; Savari et al., 2021; Sheikh et al., 2022). In this study, a neutrally buoyant resin tracer (~300 μm) radio-labelled with ^{18}F, was used to track the space–time trajectory of water inside a stirred vessel at ambient temperature (~20 °C), as illustrated in Fig. 1. In a typical PEPT experiment, the tracer is made neutrally buoyant by adding salt to

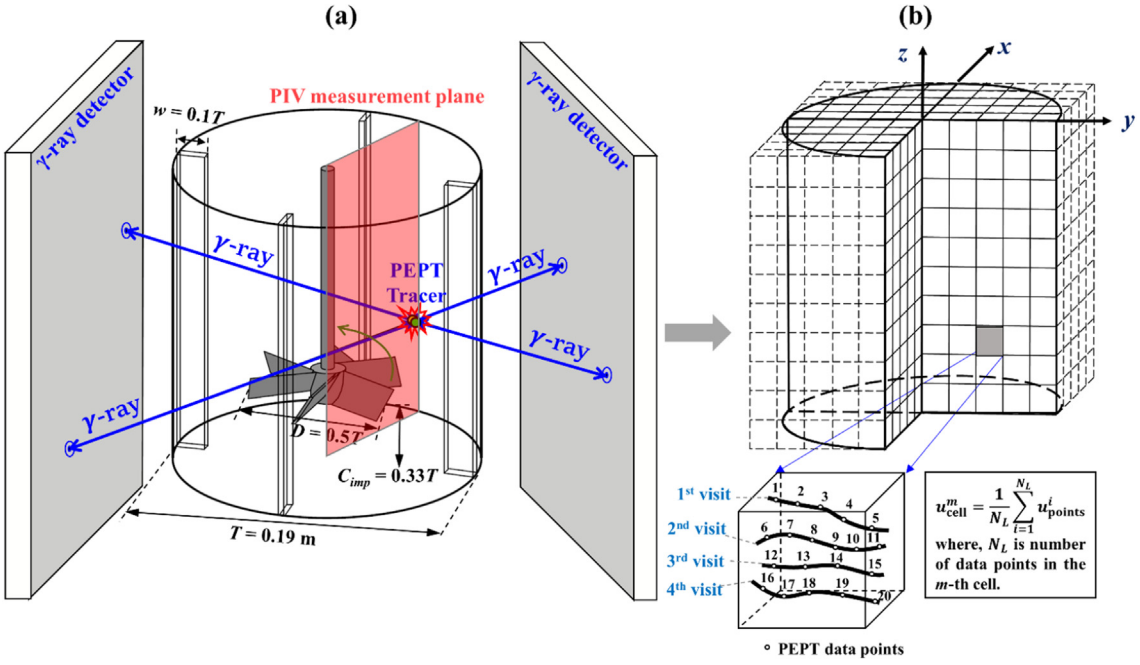

Fig. 1. (a) Experimental setup for PEPT and PIV measurements; (b) Cartesian grid mesh used for PEPT Lagrangian data analysis.

adjust the density of water so that it matches that of the tracer (1150 kg/m^3). The 3D Lagrangian trajectory was recorded for a period of 6.5 h to obtain a large number of particle locations in the tank domain and enhance data statistics. Nonetheless, using shorter tracking times yielded a similar level of accuracy, as shown in Figs. S2 and S3 in Supplementary Material; for the minimum tracking time of 30 min typically used in PEPT tracking experiments, the maximum relative difference in the global TKE value is only about 10%.

2.3. PIV experiments

In 2D PIV measurements, coated silver particles (10 μm) were suspended in the working fluid (water) and then illuminated using a laser with dual head Nd:YAG (New Wave Research, Fremont, USA). A single frame-straddling charge-coupled device (CCD) camera (TSI PowerView Plus, USA) was used to capture 15 image pairs per second. The resolution of images was 2048 × 2048 pixels^2 and a TSI LASERPLUS 610,035 synchronizer was used to control the laser and camera. The images were split into 16 × 16 pixels^2 interrogation areas each measuring 1.04 × 1.04 mm^2. The captured images were processed by a recursive Nyquist grid. Fast Fourier transform cross correlation was used to interrogate the pairs of images by TSI Insight software. The same vessel used for PEPT experiments was utilised for PIV measurements at ambient temperature (∼20 °C). The laser plane was used to conduct measurements in vertical planes at azimuthal positions of 5°, 45° and 85° from the nearest baffle (Fig. 1). The glass mixing vessel was located inside a water filled square-section tank (also made of glass) to minimise light distortion. Other software and hardware details of the measurements and associated data analysis and protocols are described in our previous work (Guida et al., 2010a).

3. Theory and data analysis

3.1. Lagrangian trajectory decomposition

The Lagrangian trajectory of the PEPT tracer consists of deterministic and stochastic parts. Let the x-direction of the trajectory be represented by the $x(t)$ time series which can be written as a sum of its low frequency (deterministic) $x_{det}(t)$ and high frequency (stochastic) $x_{sto}(t)$ displacements of the tracer, thus:

$$x(t) = x_{det}(t) + x_{sto}(t) \tag{1}$$

These two components can be separated using the wavelet analysis technique. The wavelet transform is an effective decomposition transform which provides precise frequency information at both high and low frequencies. In this work, the discrete wavelet transform which has been extensively used in the field of digital signal processing, is used to decompose the position time series into multiple frequency bands, and is defined as (Sundararajan, 2016):

$$DWT(j,k) = \frac{1}{\sqrt{\left|2^j\right|}} \int x(t)\psi\left(\frac{t - k.2^j}{2^j}\right)dt \tag{2}$$

where, ψ is the mother wavelet function, j and k are the scale and time lag coefficients, respectively. Mallat (1989) proposed an efficient algorithm for an orthogonal wavelet transform by passing the input time series through a set of low-pass and high-pass filters. While passing through these filters, the frequency resolution is doubled at each level of the decomposition, and the time resolution is halved through down-sampling. The decomposed sub-signal at the j-th scale is composed of an approximation $A_j(t)$ and a detail sub-signal $D_j(t)$. The detail and approximation components at j-level, lie within a frequency band of $[2^{-(j+1)}f_s,\ 2^{-j}f_s]$ and $[0,\ 2^{-(j+1)}f_s]$, respectively, where f_s is the time series sampling frequency. As a result, the original time series $x(t)$ can be reconstructed from the decomposed sub-signals, thus:

$$x(t) \approx A_{j,x}(t) + D_{j,x}(t) + D_{j-1,x}(t) + \cdots + D_{1,x}(t) j = 1,2,3,\cdots,J \tag{3}$$

This decomposition can also be applied to the y- and z-direction time series giving a multiresolution representation of the 3D Lagrangian tracer trajectory. As shown in Fig. 2, by considering the decomposed sub-x, y and z signals, two Lagrangian sub-trajectories, deterministic and stochastic, are reconstructed which can be used to study flow dynamics in lieu of the original trajectory. This is called multiscale or multiresolution decomposition of the trajectory, which allows the flow trajectory to be investigated at different scales.

3.2. Analysis of flow dynamics

3.2.1. Instantaneous, mean and fluctuating velocity fields

The original and decomposed Lagrangian PEPT trajectories can be used to calculate the mean and fluctuating flow velocity fields. The instantaneous and background velocities (i.e., mean flow) can be calculated from the time derivative of the original and deterministic trajectories, respectively:

$$\boldsymbol{u} = u_x\boldsymbol{e}_x + u_y\boldsymbol{e}_y + u_z\boldsymbol{e}_z = \frac{dx}{dt}\boldsymbol{e}_x + \frac{dy}{dt}\boldsymbol{e}_y + \frac{dz}{dt}\boldsymbol{e}_z \tag{4}$$

$$\bar{\boldsymbol{u}} = \bar{u}_x\boldsymbol{e}_x + \bar{u}_y\boldsymbol{e}_y + \bar{u}_z\boldsymbol{e}_z = \frac{d\bar{x}}{dt}\boldsymbol{e}_x + \frac{d\bar{y}}{dt}\boldsymbol{e}_y + \frac{d\bar{z}}{dt}\boldsymbol{e}_z$$

where, t is time and $\boldsymbol{e}_x$, $\boldsymbol{e}_y$, and $\boldsymbol{e}_z$ are unit vectors. Thus, a Lagrangian data set $[t, x, y, z, u_x, u_y, u_z, \bar{u}_x, \bar{u}_y, \bar{u}_z]$ can be generated. The time derivatives in each direction can be estimated using a differencing method and the ratio of position to time. The fluctuating Lagrangian velocity at each point is the difference between the mean and instantaneous velocities, thus, the fluctuating velocity data set $[t, x, y, z, u'_x, u'_y, u'_z]$ can be calculated. The Eulerian flow fields can be constructed from the Lagrangian data using a 3D Cartesian mesh, as shown in Fig. 1. The local velocity values in each cell are calculated by averaging the velocities at all particle data points along trajectory segments corresponding to different tracer visits inside the cell.

3.2.2. Turbulent kinetic energy

Turbulent kinetic energy is one of the key turbulence properties in the design of mixing systems and refers to the mean kinetic energy contained within eddies in the flow. In the Reynolds-averaged Navier–Stokes approach, the turbulence velocity field is split into average and instantaneous velocity fields and a time average is used to extract the mean flow properties. This can be performed using the ensemble-averaged velocity:

$$u_i = \bar{u}_i + u'_i \tag{5}$$

where, u_i, $\bar{u}_i$ and u'_i are instantaneous, time-averaged and fluctuating components in the i-direction, respectively. A similar decomposition can be implemented for angle-resolved velocity data (Sharp and Adrian, 2001), thus:

$$u_i = \bar{u}_i\Big|_\theta + u''_i \tag{6}$$

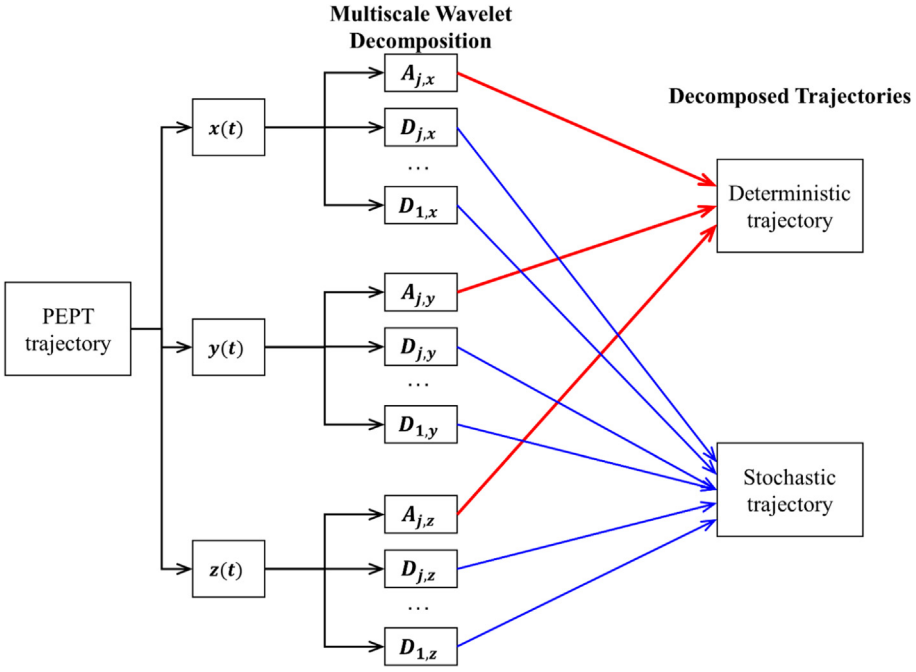

Fig. 2. Flow diagram of multiscale wavelet decomposition of Lagrangian PEPT trajectory.

where, $\bar{u}_i\big|_\theta$ is the angle-resolved averaged velocity. For mechanically agitated vessels, the velocities near the rotating impeller fluctuate in different ways: some are purely turbulent, while others are caused by the periodic motion of the impeller. The latter fluctuations behave differently from pure turbulence and must, therefore, be accounted for in a distinct way. The periodic fluctuations in angle-resolved velocity data can be determined as:

$$u_p = \bar{u}_i\big|_\theta - \bar{u}_i \tag{7}$$

Because the fluctuating part should only consist of pure random fluctuations caused by turbulence, the periodic component in the flow should be removed. Hence, the pure or random fluctuations for angle-resolved velocity data are obtained from:

$$u_i'' = u_i' - u_p \tag{8}$$

Rigorous calculation of TKE, k, needs all three fluctuating velocity components to be known, such that:

$$k = \frac{1}{2}\left(\overline{u_x'^2} + \overline{u_y'^2} + \overline{u_z'^2}\right) \tag{9}$$

Thus, the TKE at each Lagrangian data point can be estimated from Eq. (9), using the fluctuating Lagrangian velocities inferred in each direction.

For 2D PIV where only two velocity components are measured, k is usually estimated using a pseudo-isotropic approximation, as follows:

$$k = \frac{3}{4}\left(\overline{u_x'^2} + \overline{u_y'^2}\right) \tag{10}$$

This approximation has been used by many researchers and was verified by Khan et al. (2006) for mixing tanks by stereoscopic PIV data.

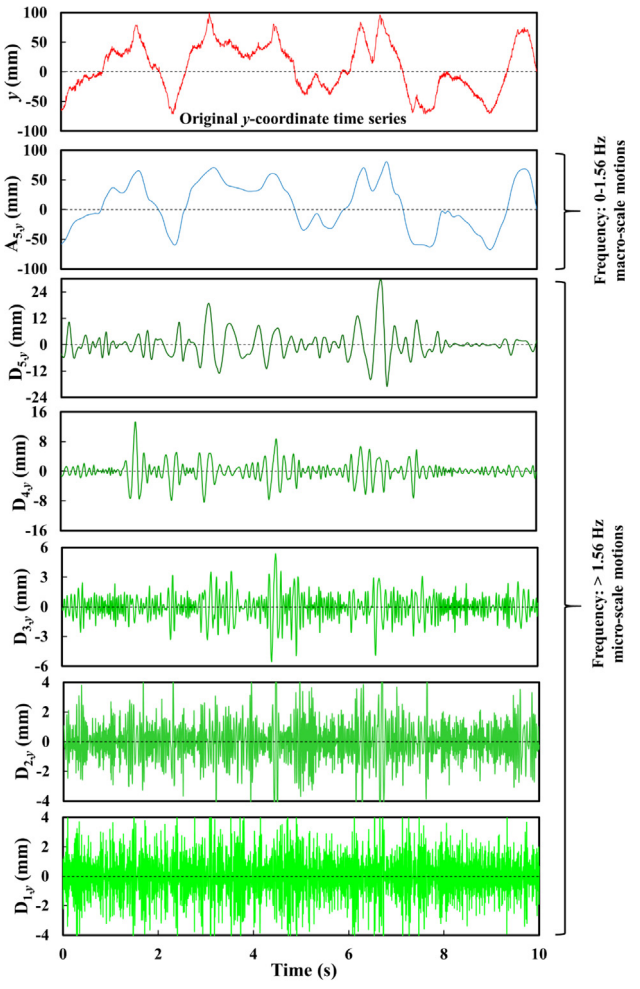

Fig. 3. Example of y-coordinate decomposed trajectory sub-signals.

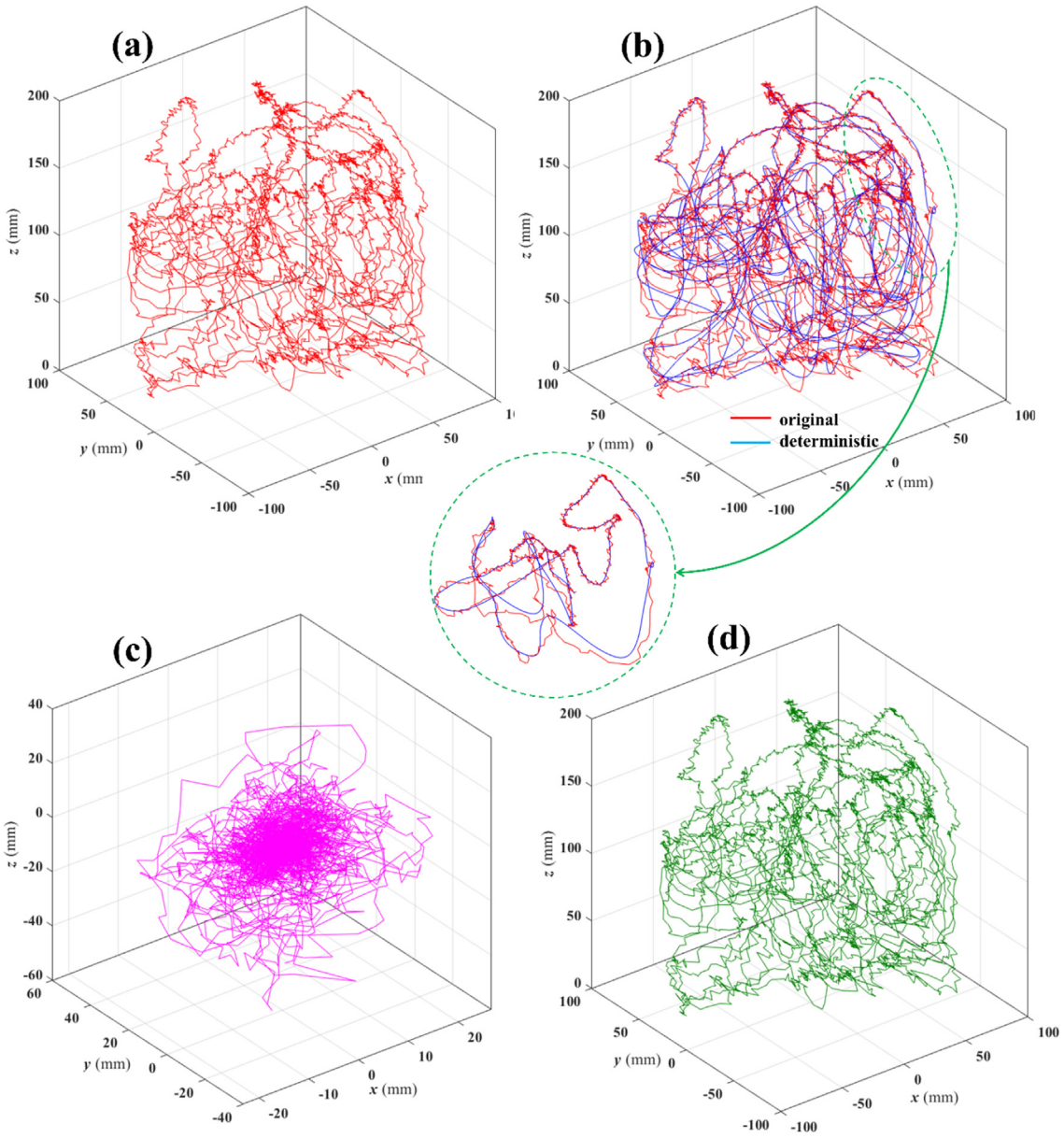

Fig. 4. Illustration of (a) original, (b) deterministic superimposed on original and (c) stochastic trajectories in the *y*-direction, yielding (d) reconstructed 3D Lagrangian trajectory.

3.2.3. Turbulent kinetic energy dissipation rate

In mixing tanks, the input turbulent kinetic energy is converted into heat through viscous dissipation and eddy generation. The TKE dissipation rate reflects the micromixing intensity in the system and is a key property for quantifying turbulence intensity in the flow. It can be evaluated from the kinematic viscosity (ν) and fluctuating velocity gradients based on the Reynolds-averaged TKE equation (Hinze, 1967):

$$\varepsilon = \nu \left\{ \begin{array}{l} 2\overline{\left(\frac{\partial u_x'}{\partial x}\right)^2} + \overline{\left(\frac{\partial u_y'}{\partial x}\right)^2} + \overline{\left(\frac{\partial u_z'}{\partial x}\right)^2} + \overline{\left(\frac{\partial u_x'}{\partial y}\right)^2} \\ +2\overline{\left(\frac{\partial u_y'}{\partial y}\right)^2} + \overline{\left(\frac{\partial u_z'}{\partial y}\right)^2} + \overline{\left(\frac{\partial u_x'}{\partial z}\right)^2} + \overline{\left(\frac{\partial u_y'}{\partial z}\right)^2} \\ +2\overline{\left(\frac{\partial u_z'}{\partial z}\right)^2} + 2\left(\overline{\left(\frac{\partial u_x'}{\partial y}\right)\left(\frac{\partial u_y'}{\partial x}\right)} + \overline{\left(\frac{\partial u_x'}{\partial z}\right)\left(\frac{\partial u_z'}{\partial x}\right)} + \overline{\left(\frac{\partial u_y'}{\partial z}\right)\left(\frac{\partial u_z'}{\partial y}\right)}\right) \end{array} \right\} \quad (11)$$

Since PEPT experimental data provides three velocity components, all fluctuating velocity gradients in the equation can be calculated using a 3D Cartesian mesh, as illustrated in Fig. 1. The local TKE dissipation rates can be determined in each cell using the average of fluctuating velocity components and dividing by the cell width.

3.2.4. Turbulent diffusion coefficients

Mass transfer within a moving fluid takes place via two mechanisms, i.e., advection which is defined by the mean fluid motion, and diffusion defined by the random motion of species and Brownian motion of molecules. The conservation of species in 3D Cartesian coordinates is (Bird et al., 2007):

$$\frac{\partial c}{\partial t} + u_x\frac{\partial c}{\partial x} + u_y\frac{\partial c}{\partial y} + u_z\frac{\partial c}{\partial z} = D_m\left(\frac{\partial^2 c}{\partial x^2} + \frac{\partial^2 c}{\partial y^2} + \frac{\partial^2 c}{\partial z^2}\right) \quad (12)$$

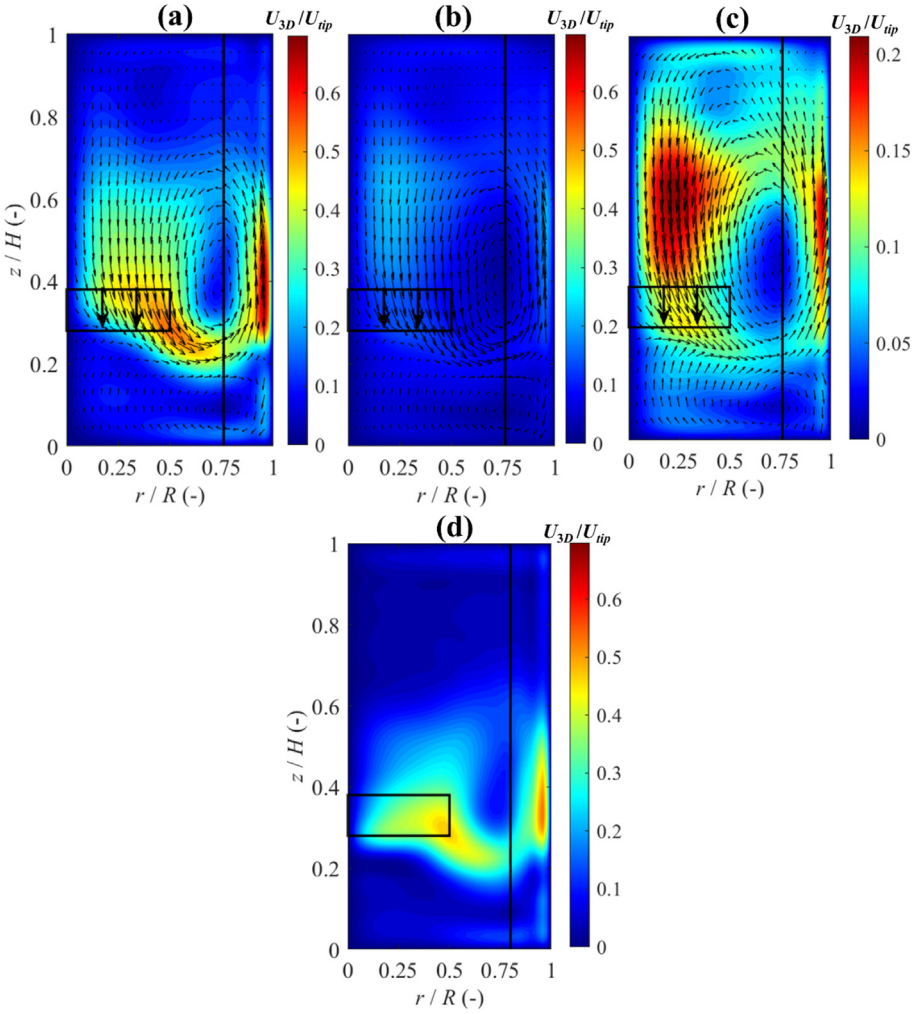

Fig. 5. Contours of azimuthally-averaged total velocity superimposed on *r*-*z* velocity vector plots: (a) original, (b) background, (c) enlarged background, (d) stochastic flow maps obtained from Lagrangian PEPT trajectories.

where, c and D_m are species concentration and molecular diffusion coefficient, respectively. In turbulent flow, the instantaneous concentration can be decomposed into mean and fluctuation components:

$$c = \bar{c} + c' \tag{13}$$

Substituting Eq. (13) into Eq. (12) and using $\overline{u_x'c'} = -K_x \frac{\partial \bar{c}}{\partial x}$, $\overline{u_y'c'} = -K_y \frac{\partial \bar{c}}{\partial y}$ and $\overline{u_z'c'} = -K_z \frac{\partial \bar{c}}{\partial z}$, gives the advection–diffusion equation for turbulent flow:

$$\frac{\partial \bar{c}}{\partial t} + \bar{u}_x \frac{\partial \bar{c}}{\partial x} + \bar{u}_y \frac{\partial \bar{c}}{\partial y} + \bar{u}_z \frac{\partial \bar{c}}{\partial z} = D_m \left(\frac{\partial^2 \bar{c}}{\partial x^2} + \frac{\partial^2 \bar{c}}{\partial y^2} + \frac{\partial^2 \bar{c}}{\partial z^2} \right) + \frac{\partial}{\partial x}\left(K_x \frac{\partial \bar{c}}{\partial x} \right) + \frac{\partial}{\partial y}\left(K_y \frac{\partial \bar{c}}{\partial y} \right) + \frac{\partial}{\partial z}\left(K_z \frac{\partial \bar{c}}{\partial z} \right) \tag{15}$$

where, K_i is the turbulent or eddy diffusivity coefficient in the i-direction. The left-hand side term represents advection transport, whilst the first term on the right-hand side represents diffusion transport and the last three terms express turbulent diffusion transport. The turbulent diffusion coefficients play an important role in turbulent flow mixing as they control micromixing.

Here, the decomposed Lagrangian PEPT trajectory provides an unprecedented opportunity to estimate turbulent diffusion coefficients in mechanically agitated vessels. They can be estimated by combining turbulence and mixing length theory (Obukhov, 1941). In this way, based on the analogy with the kinetic theory of gases, the contribution of eddy diffusivity due to velocity fluctuations is considered proportional to the product of the corresponding '*mixing length*' and the '*characteristic velocity scale*' of the fluctuations. Okubo and Ebbesmeyer (1976) further suggested that the local mixing length and characteristic velocity scale can be approximated, respectively, by the standard deviation of the Lagrangian stochastic displacement and the fluctuating velocity components. Hence, the turbulent diffusion coefficients can be expressed, thus:

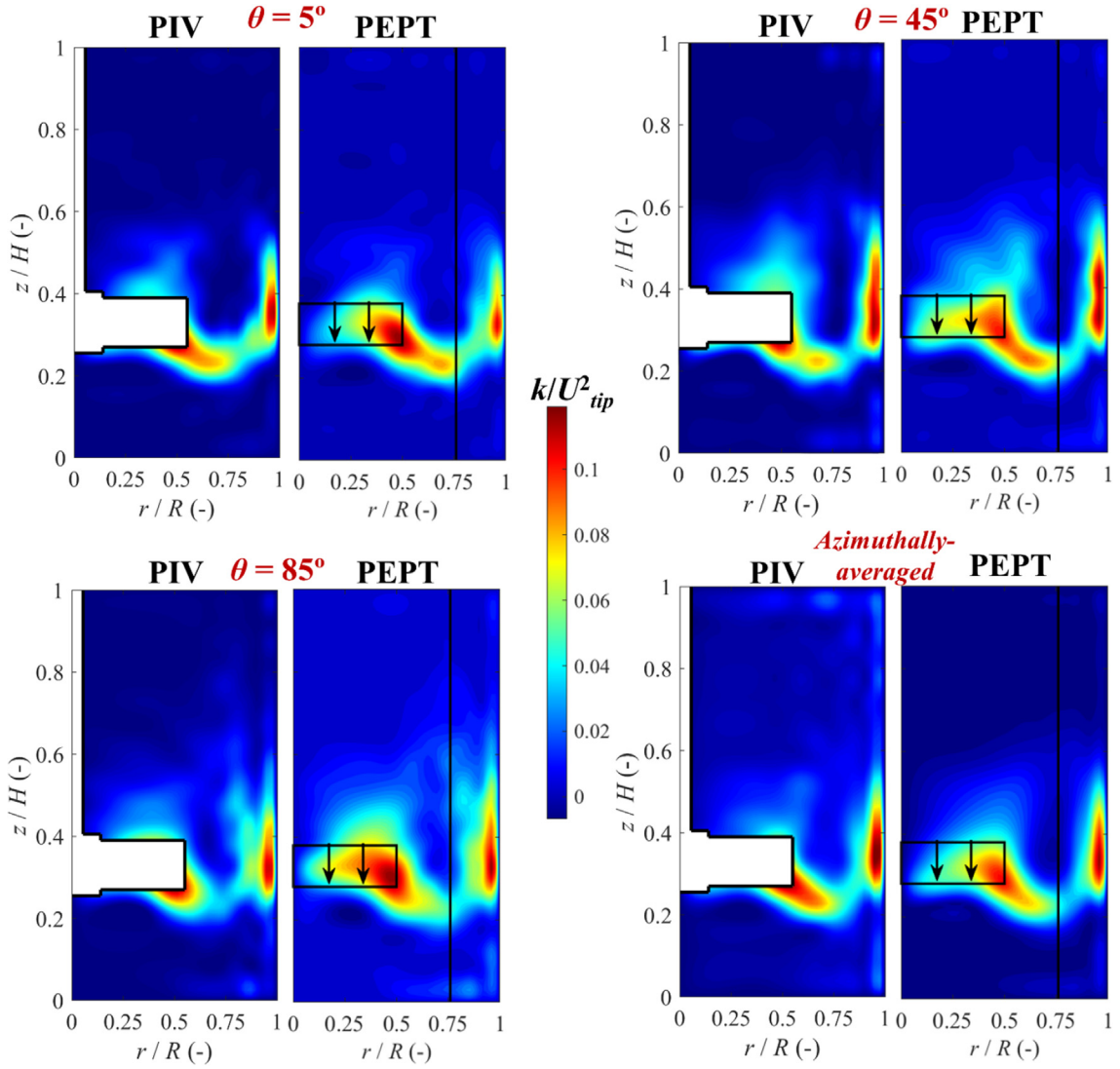

Fig. 6. Comparison of 2D contour maps of normalized TKE inferred from PIV and PEPT measurements in different azimuthal θ -planes of the same mixing vessel.

$$K_x = b\sigma_x\delta_x, \quad K_y = b\sigma_y\delta_y, \quad K_z = b\sigma_z\delta_z \tag{16}$$

where, b = 0.1, and σ and δ are standard deviations of Lagrangian stochastic displacement and fluctuating velocity components, respectively. This model has been used and validated in different mixing studies of oceanography (Ivanov and Chu, 2019; Ivanov et al., 2021; LaCasce, 2008; Monin and Yaglom, 2013).

4. Results and discussion

4.1. Mean and random trajectories

In theory, the maximum wavelet decomposition level can be calculated as $\log_2(n)$, where n is the length of the given time series. The higher the decomposition level, the more sub-signals and detailed information of the time series can be acquired. There is no general way for choosing an appropriate decomposition level as this depends on the purpose of the analysis and the process at hand. In this study, the appropriate decomposition level was determined by comparing the TKE calculated from decomposed PEPT Lagrangian trajectories to that obtained from PIV measurements, as discussed further below in section 4.3. It turned out that the best agreement between TKE from PEPT and TKE from PIV corresponded to 5 levels of decomposition.

For illustration purposes, the original and decomposed sub-signals for 10 s of the trajectory in the y-direction are shown in Fig. 3. The original signals can be decomposed into six signal components on different frequency bands after the five levels of decomposition. Two different scales can be extracted from the decomposed sub-signals, i.e., macro or low frequency scale (0–1.56 Hz) represented by approximate sub-signal $A_{5,y}$, and micro or high frequency scale (>1.56 Hz) represented by detail sub-signals $D_{1,y}$, $D_{2,y}$, $D_{3,y}$, $D_{4,y}$ and $D_{5,y}$. Thus, for each coordinate, a mean (deterministic) and stochastic signal can be constructed using $A_{5,y}$ and $D_{1,y} + D_{2,y} + D_{3,y} + D_{4,y} + D_{5,y}$, respectively. The original, mean, stochastic and reconstructed 3D Lagrangian trajectories corresponding to signals from Fig. 3 are shown in Fig. 4. It is worth noting that the reconstructed 3D trajectory has been rebuilt by combining the A_5 and D_1-D_5 sub-signals. As can be seen from Fig. 4b, the mean or background component of the trajectory is very similar to the original one in Fig. 4a, but with a smooth tracer movement representing the flow motion at the largest scales, i.e., advection without the smaller fluctuations. The stochastic trajectory (Fig. 4c) which represents the fluctuation parts of the original

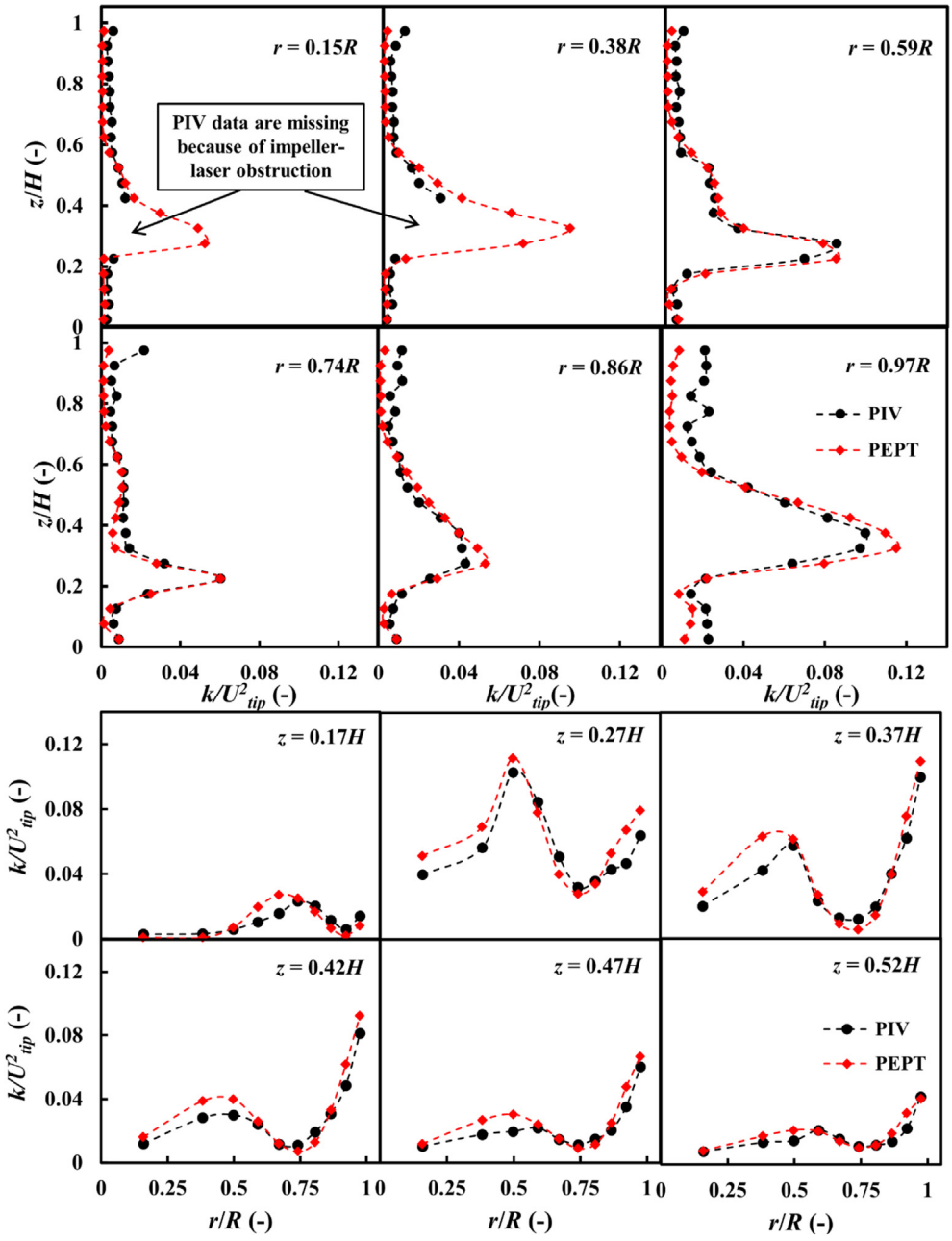

Fig. 7. Comparison of azimuthally-averaged 2D axial and radial distributions of normalized TKE inferred from PIV and PEPT measurements in the same mixing vessel.

trajectory reflects the smallest scales of the fluid flow (i.e., eddy and molecular diffusion). The reconstructed trajectory obtained by combining the mean and stochastic parts (Fig. 4b and Fig. 4c) is presented in Fig. 4d and is superimposed on the original trajectory (Fig. 4a). The original and reconstructed trajectories coincide exactly, given that the reconstructed error between the two trajectories is 1.5×10^{-8} mm which is vanishingly small, proving that the decomposition process is reliable and introduces no significant errors.

4.2. Flow velocity maps

As discussed in section 3.2.1, Lagrangian trajectories can be converted to Eulerian velocity maps using an equal volume mesh grid. Such velocity maps are usually presented as azimuthally-averaged and normalized by the impeller tip velocity (U_{tip}). The Eulerian total velocity (U_{3D}) contour map and the *r-z* velocity (U_{rz}) vector plot obtained from the original PEPT trajectory are superimposed in Fig. 5a. The flow field shows a large predominant anti-clockwise flow loop above a less prominent flow loop with clockwise circulation beneath the impeller, which is typical of flow in tanks stirred with a down-pumping PBT impeller with a high impeller-to-tank diameter ratio as is the case here (Aubin et al., 2001; Jaworski et al., 2001). The eye of the primary circulation loop is located at an elevation $\sim 0.45H$ and a radial position at $\sim 0.75R$. The fluid above the impeller is entrained into the PBT and discharged towards the vessel wall by a high-speed oblique jet, and then slows down as it approaches the free surface. The fluid near the surface is relatively quiescent with velocities around $0.1U_{tip}$.

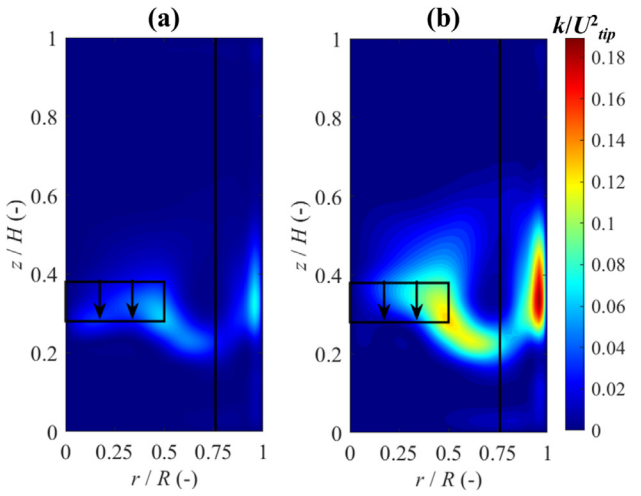

Fig. 8. Contour maps of azimuthally-averaged TKE inferred from PEPT measurements by (a) 2D and (b) 3D estimations.

The azimuthally-averaged normalized mean (background) flow velocity map superimposed over the *r-z* velocity vector plot is presented in Fig. 5b. The gross flow pattern of the mean flow is qualitatively similar to the original one, but the velocities are much smaller (Fig. 5a). The background flow map shows the primary motion of fluid in the tank and indicates mixing on the large temporal and spatial scales, i.e., macromixing characterised by the length scale of the rotating impeller. For better clarity, the same velocity map is shown enlarged in Fig. 5c. Here, macromixing prevails in the region above the impeller and near the tank wall, where the advective velocities are highest. This scale of mixing is associated with large turbulent eddies, i.e., primary circulation loop which determines the homogenization and the movement of the bulk fluid. In other words, it determines how quickly fluid disperses and blends throughout the vessel.

The azimuthally-averaged fluctuating velocity contour map is shown in Fig. 5d; the colour scale highlights the regions characterised by high velocity fluctuations. Note that no velocity vectors can be shown as the fluctuating velocities have random direction. This velocity field represents a map of the micromixing scale in the tank. Micromixing prevails in the impeller discharge stream and where the discharge stream impinges on the tank wall. This micromixing scale is governed by small eddies which are created within vortices behind the impeller blades and by the fluid jet impinging on the vessel wall. The above description is specific to the flow and mixing conditions considered here. The intensity of macro- and micromixing as well as its spatial distribution is influenced by a number of factors including mixer configuration, fluid rheology and regime of flow. A variation in any one of these parameters may impact the different mixing scales to different extents. Hence, an analysis of the sort proposed here is therefore very useful for unravelling these phenomena.

4.3. TKE maps

The decomposed 3D Lagrangian PEPT trajectories were used to estimate local TKE values within the vessel. To independently validate these TKE estimations, PIV measurements obtained in the same vessel were used. It should be noted that 2D PIV has been shown to give accurate measurements of turbulence properties compared to LDV and hot-wire anemometry (Gagnon et al., 2008; Lavoie et al., 2007; Saarenrinne et al., 2001). Since PIV data are 2D, TKE values were estimated from Eq. (10) for both PIV and PEPT using the same 2D approach. The 2D TKE contour maps estimated from PEPT and PIV, normalized by the square of the impeller tip velocity (k/U^2_{tip}) are compared in Fig. 6. Results are presented in different sample azimuthal planes, i.e., θ = 5°, 45°, 85°, and an average contour of 17 such azimuthal planes is also shown. In addition, for a more detailed quantitative comparison, azimuthally-averaged axial and radial TKE distributions are depicted in Fig. 7, in planes of particularly high TKE values, i.e., z = 0.17, 0.27, 0.37, 0.42, 0.47, 0.52H; and r = 0.15, 0.38, 0.59, 0.74, 0.86, 0.97R.

A sensitivity analysis of TKE values to the number of levels used in the decomposition of PEPT trajectories showed that 5 levels gave the closest agreement with PIV, as depicted in Fig. S1 in Supplementary Material. A smaller number of decomposition levels favours large scale advection, thus, underestimating TKE; whereas, with a higher level, small scale fluctuations are overrepresented, thereby overestimating TKE. Comparison of the PIV and PEPT results indicates that TKE magnitude and its spatial distribution are in good agreement (Figs. 6 and 7). Slight discrepancies exist near the tip of the impeller and close to the tank wall where the estimations yielded by PEPT are slightly higher than those obtained from PIV. These results give useful insight into the distribution of TKE within the stirred vessel. The highest TKE values appear in the impeller discharge stream and where it impinges on the vessel wall, caused by trailing vortices behind the impeller blades.

As discussed above, the use of 2D data to estimate TKE assumes pseudo-isotropic turbulence, which seems to be unrealistic in a 3D mixing flow. Here, 3D PEPT Lagrangian data provides an unprecedented opportunity to check this assumption in stirred tanks. Thus, TKE values estimated from PEPT trajectories based on 2D approximation (Eq. (10) and based on 3D calculations (Eq. (9)) are compared in Figs. 8 and 9, respectively, on the basis of contour plots and azimuthally-averaged axial and radial distributions. The contour maps in Fig. 8 based on 2D and 3D estimations are similar except for locations in the impeller discharge stream and opposite the impeller at the wall. The quantitative distributions in Fig. 9, however, generally show some small discrepancies between the two sets of data, with the 2D profiles underestimating TKE. The most significant differences appear just above the impeller and in the impeller plane, increasing as the discharge flow approaches the wall. Apart from these latter strongly anisotropic regions, the generally fair agreement between the 2D and 3D distributions shows that in most parts of the vessel the assumption of pseudo-isotropic turbulence is reasonable.

4.4. TKE dissipation rate maps

A 2D contour map of azimuthally-averaged TKE dissipation rate estimated from PEPT data and normalized by N^3D^2, is superimposed over the *r-z* velocity vector plot in Fig. 10. The dissipation rate is highest between the blades within the impeller volume and decreases gradually as the discharge stream approaches the vessel wall. The fluid in the bulk of the tank has a very low dissipation rate, an order of magnitude lower. Thus, the vast majority of the TKE is dissipated within the impeller, which represents only a small fraction of the vessel volume.

To verify the TKE dissipation rate estimations, the local ε values were integrated over the grid shown in Fig. 1 to yield the average dissipation rate in the tank, as $\bar{\varepsilon} = 0.13$ m^2/s^3. Using the well-established value of 2.0 for the power number ($N_p = P/\rho N^3 D^5$) of the PBT impeller (Liu and Barigou, 2013), the power input P was

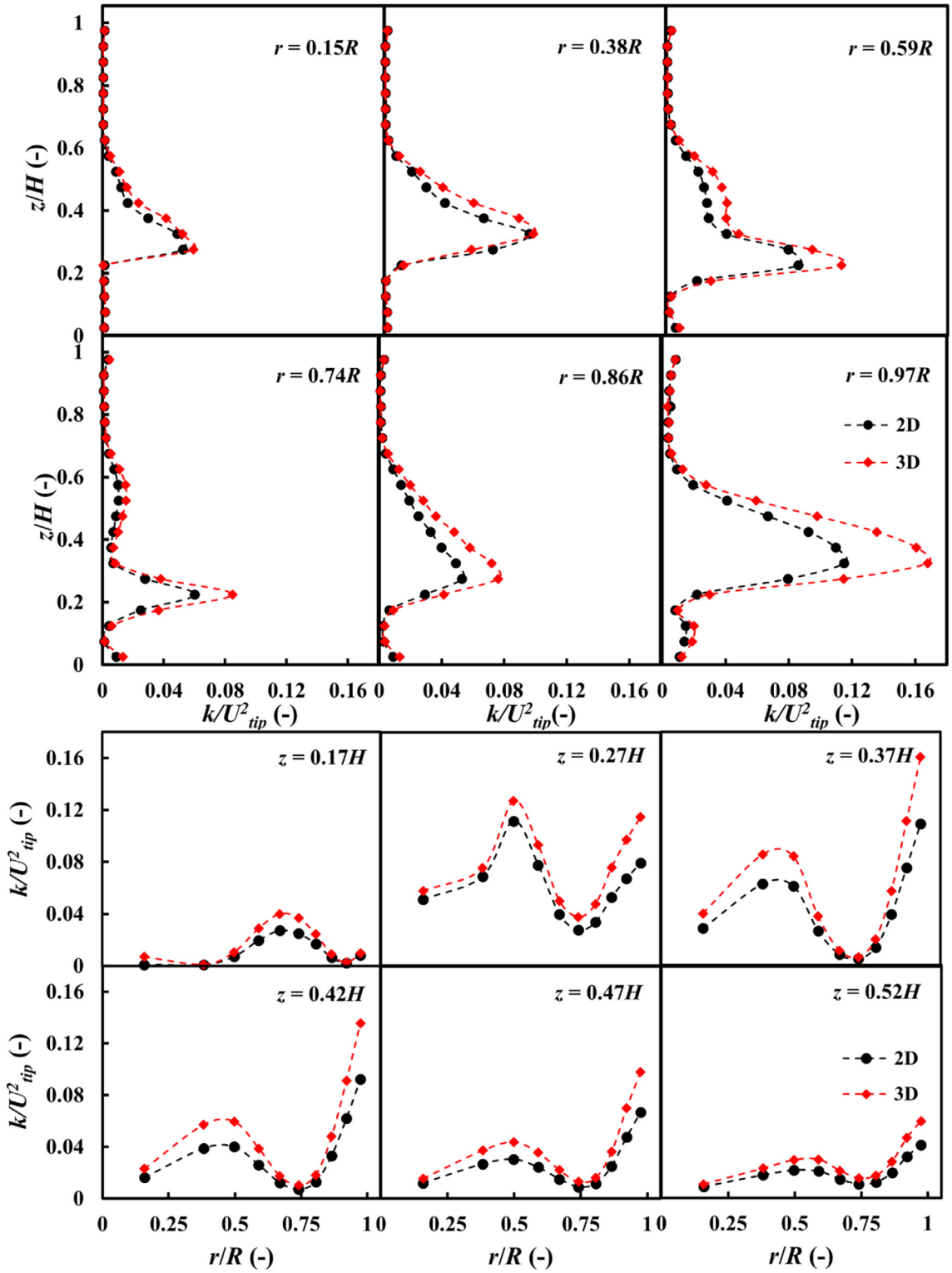

Fig. 9. Azimuthally-averaged axial and radial distributions of TKE inferred from PEPT measurements by 2D and 3D estimations.

obtained and, hence, the mean dissipation rate was estimated, thus, $\bar{\varepsilon} = P/(\rho V_l) = 0.14\ m^2/s^3$, where V_l is liquid volume in the vessel. The close agreement of the two estimated values of $\bar{\varepsilon}$ confirms the accuracy of the TKE dissipation rate estimations.

4.5. Turbulent diffusion coefficients maps

The 3D PEPT trajectories enabled for the first time the estimation of the turbulent diffusion coefficients in a stirred vessel. 2D

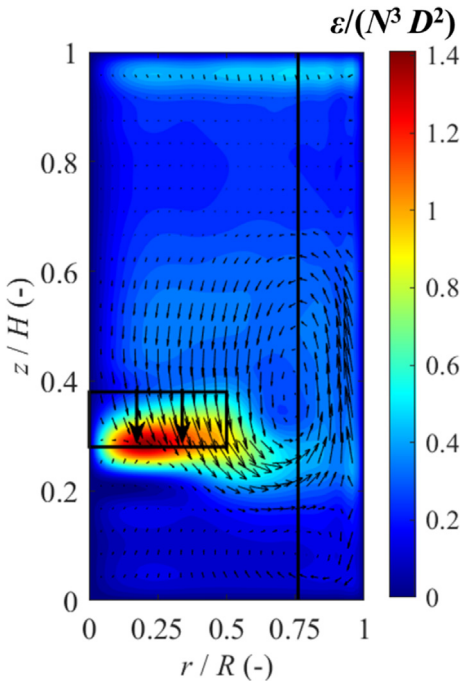

Fig. 10. Contour map of azimuthally-averaged TKE dissipation rate superimposed on *r-z* velocity vectors.

contour maps of the azimuthally-averaged values estimated from PEPT data are superimposed over *r-z* velocity vector plots in Fig. 11, while their axial and radial distributions are presented in Fig. 12. The radial diffusion coefficient (K_y) exhibits some of the largest values compared with K_x and K_z. K_x which represents tangential turbulence has its highest values within the impeller volume, and so turbulent diffusion in the *x*-direction is predominant in this region. The radial K_y coefficient exhibits its largest values in the impeller discharge stream where turbulent diffusion appears to be predominant in the radial direction. On the other hand, the axial coefficient K_z attains its largest magnitude where the discharged stream impinges on the vessel wall and in the region above the impeller, indicating that turbulent diffusion in these areas is predominant axially. The average value of these coefficients within the vessel is on order of 10^{-4} m^2/s which is $\sim 10^5$ times the typical molecular diffusion coefficient in water (Perry et al., 1997). This indicates that micromixing in turbulent stirred tanks are completely controlled by turbulent eddy diffusion.

5. Conclusion

A discrete wavelet transform was used to decompose experimental 3D Lagrangian PEPT flow trajectories into their deterministic and fluctuating components in a turbulent mechanically agitated vessel and provide a pointwise description of the mean and fluctuation velocities, TKE and its dissipation rate as well as turbulent diffusion coefficients. The deterministic component accounts for low frequency scale motion, i.e., non-diffusive or background motion, while the stochastic component represents high frequency scale motion, i.e., diffusive motion of small eddies. The analysis was independently validated via 2D PIV measurements.

Background flow represents the primary fluid motion in the bulk of the tank and prevails in the region above the impeller and near the tank wall, where the highest axial velocities occur. Fluctuating flow, which is governed by small eddies, however, is predominant in the discharge stream and where the discharge stream impinges on the tank wall. The primary circulation loop in the vessel contains a high level of TKE which is mainly attributed to the trailing vortices in the flow loop created by the wake of the impeller blades. TKE values inferred from 2D PIV measurements are slightly lower than those rigorously estimated from 3D PEPT data. The most significant differences appear just above the impeller and in the impeller plane, increasing as the discharge flow approaches the wall. Apart from these latter strongly anisotropic regions, the generally fair agreement between the 2D and 3D distributions shows that in most parts of the vessel the assumption of pseudo-isotropic turbulence is reasonable.

The proposed wavelet analysis enabled estimation of the turbulent diffusion coefficients for the first time. Eddy diffusivities in different directions are prevalent in different regions of the

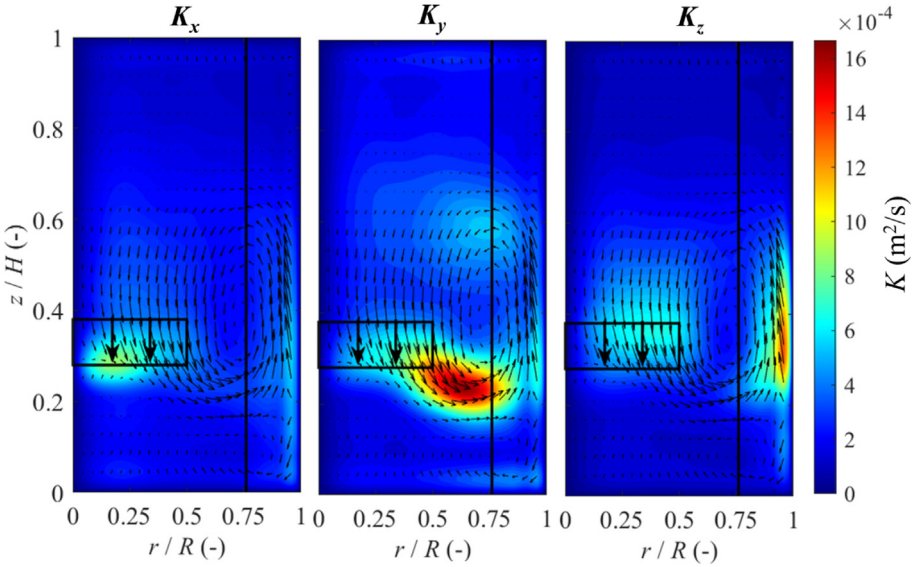

Fig. 11. Contour maps of azimuthally-averaged turbulent diffusion coefficients superimposed on *r-z* velocity vectors.

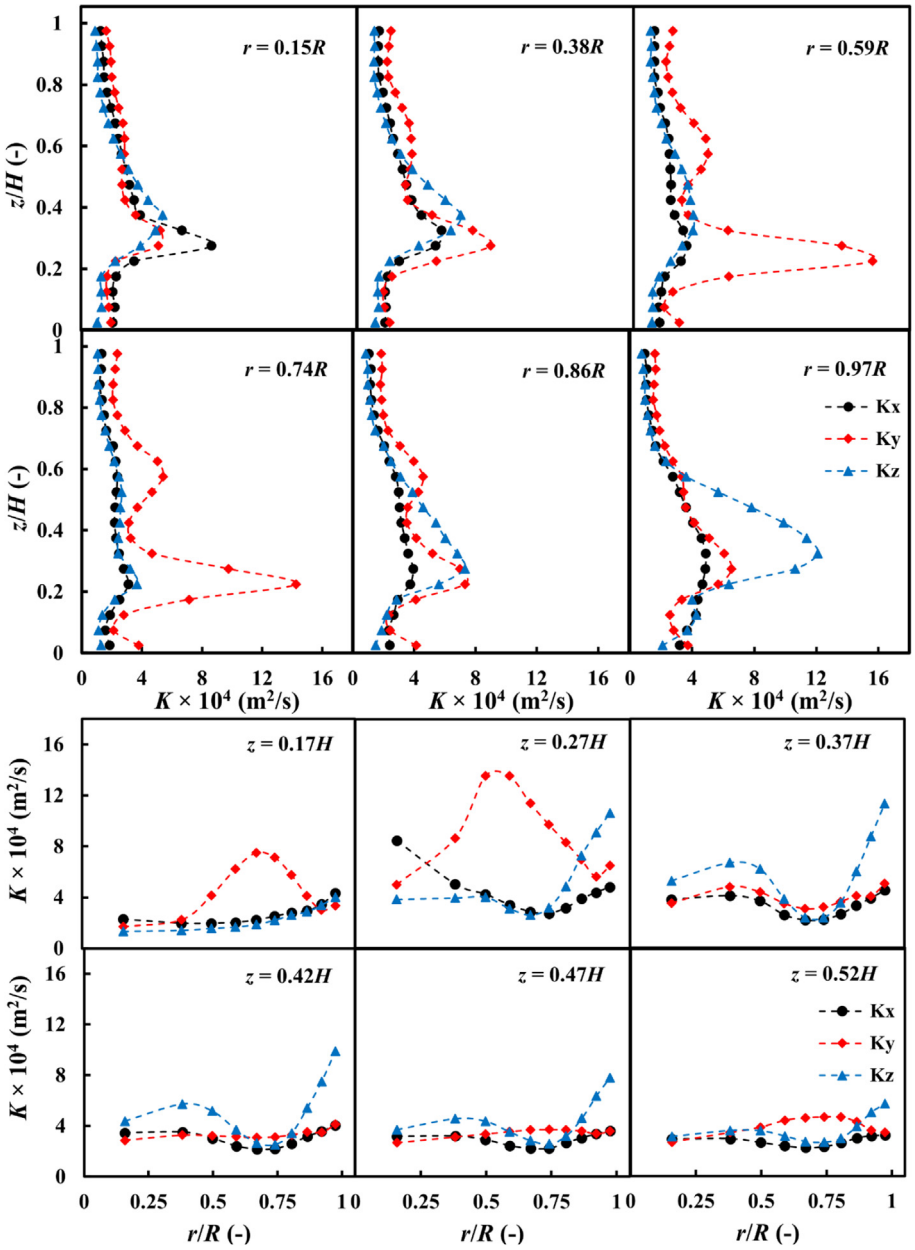

Fig. 12. Azimuthally-averaged axial and radial distributions of turbulent diffusion coefficients.

tank. K_x has high values within the impeller volume, while the highest K_y values are located in the impeller discharge stream. Axial K_z coefficient exhibits high values in the discharged plane where fluid impinges on the vessel wall and in the region above the impeller. The values of turbulent diffusion coefficients obtained show that micromixing in turbulent stirred vessels is completely controlled by turbulent eddy diffusion rather than molecular diffusion.

CRediT authorship contribution statement

Chiya Savari: Conceptualization, Methodology, Validation, Investigation, Formal analysis, Visualization, Writing – original draft. **Kun Li:** Validation, Visualization, Writing – review & editing. **Mostafa Barigou:** Conceptualization, Methodology, Supervision, Funding acquisition, Writing – review & editing.

Data availability

The authors decline to share data

Declaration of Competing Interest

The authors declare that they have no known competing financial interests or personal relationships that could have appeared to influence the work reported in this paper.

Acknowledgement

This work was supported by EPSRC Programme Grant EP/R045046/1: Probing Multiscale Complex Multiphase Flows with Positrons for Engineering and Biomedical Applications (PI: Prof. M. Barigou, University of Birmingham).

Appendix A. Supplementary material

Supplementary data to this article can be found online at https://doi.org/10.1016/j.ces.2022.117844.

References

Addison, P.S., 2017. The illustrated wavelet transform handbook: introductory theory and applications in science, engineering, medicine and finance. CRC press.

Adrian, R.J., 1991. Particle-imaging techniques for experimental fluid mechanics. Annu. Rev. Fluid Mech. 23 (1), 261–304.

Antonia, R., 2003. On estimating mean and instantaneous turbulent energy dissipation rates with hot wires. Exp. Therm Fluid Sci. 27 (2), 151–157.

Argoul, F., Arneodo, A., Grasseau, G., Gagne, Y., Hopfinger, E.J., Frisch, U., 1989. Wavelet analysis of turbulence reveals the multifractal nature of the Richardson cascade. Nature 338 (6210), 51–53.

Aubin, J., Mavros, P., Fletcher, D.F., Bertrand, J., Xuereb, C., 2001. Effect of axial agitator configuration (up-pumping, down-pumping, reverse rotation) on flow patterns generated in stirred vessels. Chem. Eng. Res. Des. 79 (8), 845–856.

Babichev, S., Škvor, J., Fišer, J., Lytvynenko, V., 2018. Technology of gene expression profiles filtering based on wavelet analysis. International Journal of Intelligent Systems and Applications 10 (4), 1–7.

Barigou, M., 2004. Particle tracking in opaque mixing systems: An overview of the capabilities of PET and PEPT. Chem. Eng. Res. Des. 82 (9), 1258–1267.

Bird, R.B., Stewart, W.E., Lightfoot, E.N., 2007. Transport phenomena, Second ed. J. Wiley.

Boffetta, G., Romano, G., 2002. Structure functions and energy dissipation dependence on Reynolds number. Phys. Fluids 14 (10), 3453–3458.

Ducci, A., Yianneskis, M., 2005. Direct determination of energy dissipation in stirred vessels with two-point LDA. AIChE J. 51 (8), 2133–2149.

Eesa, M., Barigou, M., 2008. Horizontal laminar flow of coarse nearly-neutrally buoyant particles in non-Newtonian conveying fluids: CFD and PEPT experiments compared. Int. J. Multiph. Flow 34 (11), 997–1007.

Eesa, M., Barigou, M., 2009. CFD investigation of the pipe transport of coarse solids in laminar power law fluids. Chem. Eng. Sci. 64 (2), 322–333.

Ellis, N., Briens, L., Grace, J., Bi, H., Lim, C., 2003. Characterization of dynamic behaviour in gas–solid turbulent fluidized bed using chaos and wavelet analyses. Chem. Eng. J. 96 (1–3), 105–116.

Fairhurst, P., Barigou, M., Fryer, P., Pain, J., Parker, D., 2001. Using positron emission particle tracking (PEPT) to study nearly neutrally buoyant particles in high solid fraction pipe flow. Int. J. Multiph. Flow 27 (11), 1881–1901.

Fangary, Y.S., Barigou, M., Seville, J.P., Parker, D.J., 2002. A Langrangian study of solids suspension in a stirred vessel by Positron Emission Particle Tracking (PEPT). Chem. Eng. Technol. 25 (5), 521–528.

Gabriele, A., Tsoligkas, A., Kings, I., Simmons, M., 2011. Use of PIV to measure turbulence modulation in a high throughput stirred vessel with the addition of high Stokes number particles for both up-and down-pumping configurations. Chem. Eng. Sci. 66 (23), 5862–5874.

Gagnon, J., Iliescu, M., Ciocan, G., Deschênes, C., 2008. Experimental investigation of runner outlet flow in axial turbine with LDV and stereoscopic PIV, 24th IAHR Symposium on Hydraulic Machinery and Systems, Foz do Iguassu, Brazil, October. pp. 27-31.

Guenther, C., Breault, R., 2007. Wavelet analysis to characterize cluster dynamics in a circulating fluidized bed. Powder Technol. 173 (3), 163–173.

Guida, A., Nienow, A.W., Barigou, M., 2010a. The effects of the azimuthal position of the measurement plane on the flow parameters determined by PIV within a stirred vessel. Chem. Eng. Sci. 65 (8), 2454–2463.

Guida, A., Nienow, A.W., Barigou, M., 2010b. Shannon entropy for local and global description of mixing by Lagrangian particle tracking. Chem. Eng. Sci. 65 (10), 2865–2883.

Guida, A., Nienow, A.W., Barigou, M., 2012. Lagrangian tools for the analysis of mixing in single-phase and multiphase flow systems. AIChE J. 58 (1), 31–45.

Hinze, J., 1967. Secondary currents in wall turbulence. The Physics of Fluids 10 (9), S122–S125.

Ivanov, L., Chu, P., 2019. Estimation of turbulent diffusion coefficients from decomposition of Lagrangian trajectories. Ocean Model. 137, 114–131.

Ivanov, L.M., Collins, C.A., Margolina, T., 2021. Reconstruction of Diffusion Coefficients and Power Exponents from Single Lagrangian Trajectories. Fluids 6 (3), 111.

Jaworski, Z., Dyster, K., Nienow, A., 2001. The effect of size, location and pumping direction of pitched blade turbine impellers on flow patterns: LDA measurements and CFD predictions. Chem. Eng. Res. Des. 79 (8), 887–894.

Khan, F., Rielly, C., Brown, D., 2006. Angle-resolved stereo-PIV measurements close to a down-pumping pitched-blade turbine. Chem. Eng. Sci. 61 (9), 2799–2806.

Kresta, S.M., Wood, P.E., 1993. The flow field produced by a pitched blade turbine: characterization of the turbulence and estimation of the dissipation rate. Chem. Eng. Sci. 48 (10), 1761–1774.

La Forgia, N., Herø, E.H., Solsvik, J., Jakobsen, H.A., 2019. Dissipation rate estimation in a rectangular shaped test section with periodic structure at the walls. Chem. Eng. Sci. 195, 159–178.

LaCasce, J., 2008. Statistics from Lagrangian observations. Prog. Oceanogr. 77 (1), 1–29.

Lavoie, P., Avallone, G., De Gregorio, F., Romano, G., Antonia, R., 2007. Spatial resolution of PIV for the measurement of turbulence. Exp. Fluids 43 (1), 39–51.

Li, K., Savari, C., Barigou, M., 2022. Computation of Lagrangian coherent structures from experimental fluid trajectory measurements in a mechanically agitated vessel. Chem. Eng. Sci. 254, 117598.

Liu, L., Barigou, M., 2013. Numerical modelling of velocity field and phase distribution in dense monodisperse solid–liquid suspensions under different regimes of agitation: CFD and PEPT experiments. Chem. Eng. Sci. 101, 837–850.

Lyashenko, V., Babker, A., Kobylin, O., 2016. Using the methodology of wavelet analysis for processing images of cytology preparations.

Mallat, S.G., 1989. A theory for multiresolution signal decomposition: the wavelet representation. IEEE Trans. Pattern Anal. Mach. Intell. 11 (7), 674–693.

Monin, A.S., Yaglom, A.M., 2013. Statistical fluid mechanics, volume II: mechanics of turbulence. Courier Corporation.

Mortensen, H.H., Innings, F., Håkansson, A., 2018. Local levels of dissipation rate of turbulent kinetic energy in a rotor–stator mixer with different stator slot widths—An experimental investigation. Chem. Eng. Res. Des. 130, 52–62.

Obukhov, A., 1941. Spectral energy distribution in a turbulent flow. Izv. Akad. Nauk. SSSR. Ser. Geogr. i. Geofiz 5, 453–466.

Okubo, A., Ebbesmeyer, C.C., 1976. Determination of vorticity, divergence, and deformation rates from analysis of drogue observations, Deep Sea Research and Oceanographic Abstracts. Elsevier, 349–352.

Paul, E.L., Atiemo-Obeng, V.A., Kresta, S.M., 2003. Handbook of industrial mixing: science and practice. John Wiley & Sons.

Perry, R.H., Green, D.W., Maloney, J., 1997. Perry's Chemical Engineers' Handbook (ed.). Seventh, International edition.

Saarenrinne, P., Piirto, M., Eloranta, H., 2001. Experiences of turbulence measurement with PIV. Meas. Sci. Technol. 12 (11), 1904.

Savari, C., Sheikh, H.A., Barigou, M., 2021. Lagrangian Recurrence Tracking: A Novel Approach for Description of Mixing in Liquid and Particle-Liquid Flows. Ind. Eng. Chem. Res. 60 (50), 18501–18512.

Schäfer, M., Höfken, M., Durst, F., 1997. Detailed LDV measurements for visualization of the flow field within a stirred-tank reactor equipped with a Rushton turbine. Chem. Eng. Res. Des. 75 (8), 729–736.

Shah, R.S.S.R.E., Sajjadi, B., Raman, A.A.A., Ibrahim, S., 2015. Solid-liquid mixing analysis in stirred vessels. Rev. Chem. Eng. 31 (2), 119–147.

Sharp, K., Adrian, R., 2001. PIV study of small-scale flow structure around a Rushton turbine. AIChE J. 47 (4), 766–778.

Sheikh, H.A., Savari, C., Barigou, M., 2022. Lagrangian stochastic modelling of liquid flow in a mechanically agitated vessel. Chem. Eng. Sci. 249, 117318.

Stanislas, M., Okamoto, K., Kähler, C.J., Westerweel, J., Scarano, F., 2008. Main results of the third international PIV challenge. Exp. Fluids 45 (1), 27–71.

Sundararajan, D., 2016. Discrete wavelet transform: a signal processing approach. John Wiley & Sons.

Tanaka, T., Eaton, J.K., 2007. A correction method for measuring turbulence kinetic energy dissipation rate by PIV. Exp. Fluids 42 (6), 893–902.

Tao, B., Katz, J., Meneveau, C., 2000. Geometry and scale relationships in high Reynolds number turbulence determined from three-dimensional holographic velocimetry. Phys. Fluids 12 (5), 941–944.

Tao, B., Katz, J., Meneveau, C., 2002. Statistical geometry of subgrid-scale stresses determined from holographic particle image velocimetry measurements. J. Fluid Mech. 457, 35–78.

Thiebaut, S., Vennell, R., 2010. Observation of a fast continental shelf wave generated by a storm impacting Newfoundland using wavelet and cross-wavelet analyses. J. Phys. Oceanogr. 40 (2), 417–428.

Thomson, R.E., Emery, W.J., 2014. Data analysis methods in physical oceanography. Newnes.

Tropea, C., 1995. Laser Doppler anemometry: recent developments and future challenges. Meas. Sci. Technol. 6 (6), 605.

Wallace, J.M., Vukoslavčević, P.V., 2010. Measurement of the velocity gradient tensor in turbulent flows. Annu. Rev. Fluid Mech. 42, 157–181.

Wu, X., Yu, B., Wang, Y., 2013. Wavelet analysis on turbulent structure in drag-reducing channel flow based on direct numerical simulation. Advances in Mechanical Engineering 5, 514325.

Xiong, F., Qi, X., Nattel, S., Comtois, P., 2015. Wavelet analysis of cardiac optical mapping data. Comput. Biol. Med. 65, 243–255.

Zeff, B.W., Lanterman, D.D., McAllister, R., Roy, R., Kostelich, E.J., Lathrop, D.P., 2003. Measuring intense rotation and dissipation in turbulent flows. Nature 421 (6919), 146–149.

Zhou, G., Kresta, S.M., 1996. Impact of tank geometry on the maximum turbulence energy dissipation rate for impellers. AIChE J. 42 (9), 2476–2490.

Zhu, Y., Antonia, R., 1996. Spatial resolution of a 4-X-wire vorticity probe. Meas. Sci. Technol. 7 (10), 1492.